 FDMP, vol.2, no.4, pp.299-307, 2006

Simulation of Sloshing with the Volume of Fluid Method

M.H. Djavareshkian[1] and M. Khalili[2]

Abstract: This paper opens a new horizon on the simulation of sloshing phenomena. One of the most popular Finite Volume methods called VOF (Volume Of Fluid) method is used for tracking the flow in containers. The algorithm is tested for different fluid elevations, physical conditions in different road curves and liquid properties. The method is then validated against an analytical and another numerical solution. These comparisons show that the VOF can effectively solve the sloshing problem for different fluids and a variety of physical and geometrical conditions.

keyword: Pressure-based Method, VOF, Sloshing, Pendulum Model, Finite Volume Technique

Nomenclature

A, D	= finite difference coefficients
$\tilde{a}$	= cell face area
e, w, n, s	= east, west, north and south cell faces
E, W, N, S	= East, West, North and South center cells
F	= mass flux
I	= flux
q	= scalar flux vector
S^u	= momentum source term
T	= stress tensor
u, v	= velocity components in the x and y directions, respectively
Γ	= diffusivity coefficient
$\delta\upsilon$	= cell volume
μ	= dynamic viscosity
ρ	= density
ϕ	= scalar quantity
η, ζ	= local coordinates

1 Introduction

Every year, there are many fatal accidents associated with the role over of tanker trucks carrying fuel. The tendency to roll over is even higher when the tanker truck is partially filled and the fuel inside the tanker is free to slosh. Typically a half-empty tanker truck has ten times more tendency to role over than a passenger car. Sloshing also happens in the gas tank of automobiles, in the wing of an aircraft and in water towers during an earthquake. In these situations the liquid is exposed to external forces, as a consequence the free surface of the liquid becomes unstable and sloshing occurs. The sloshing amplifies the maximum fluid force exerted on the structures and causes instability. To understand the fluid–structure interaction during sloshing, accurate knowledge of the free surface behavior is necessary.

Until now, a lot of studies have considered sloshing (some initial important experimental studies are due to Martin and Moyce [1952] and Abramson [1966]). Amabili [1996] and Warnitchai and Pinkaew [1998] solved the sloshing problems by analytical methods and validated the results with some experiments.

Another possible way to study the problem is the Finite Element method. Aliabadi and Tezduyar [2000], Aliabadi et al [2003] and Johnson and Aliabadi [2000] used this technique in studying the free-surface movements. Another very promising method is the VOF Finite volume method introduced by Nichols and Hirt [1971, 1975], Maxwell [1977], Deville [1974], Hirt and Shannon [1968], Hirt et al [1975] and Liu Jun [1985].

In the above-mentioned works, the numerical simulation of free-surface flow problems is based on the solution of a complex set of partial differential equations governing the conservation of mass and momentum. This method is a kind of volume-tracking technique applied to a fixed Eulerian mesh. It has been used by Liu Jun [1986] for studying a variety of free surface problems. Similar techniques (Level set, front tracking method) have been developed by other researchers (see, e.g., Esmaeeli, 2005; Lappa, 2005: Jimenez et al., 2005; Hogea et al., 2005).

In this paper, the VOF method is employed for tracking the flow in containers. In this simulation, a non-orthogonal mesh with a collocated pressure-base formu-

[1] Assistant Prof., Tabriz University, Tabriz, Iran
[2] MSc. Student, Tabriz University, Tabriz, Iran

lation is used. The pendulum model is also considered. This model is a cost effective way for the simulation of sloshing. The results of this simulation for a tanker truck containing liquid fuel with different free surfaces, viscosities and densities are finally compared with other available results.

2 Governing Equations

The basic equations, which describe conservation of mass and momentum, can be expressed in Cartesian tensor form as

$$\frac{\partial \rho}{\partial t} + \frac{\partial (\rho u_j)}{\partial x_j} = 0 \tag{1}$$

$$\frac{\partial (\rho u_i)}{\partial t} + \frac{\partial (\rho u_i u_j - T_{ij})}{\partial x_j} = S_i^u \tag{2}$$

Where S_i^uincludes body forces. The stress tensor is usually expressed in terms of basic dependent variable. This term for a Newtonian incompressible fluid is

$$T_{ij} = -p\delta_{ij} + \mu(\frac{\partial u_i}{\partial x_j} + \frac{\partial u_j}{\partial x_i}) \tag{3}$$

3 Volume Of Fluid (VOF) Method

In this method, the actual location of the interface is determined by some additional computations based on the distribution of markers within each cell.

VOF is a proper method for modeling two or more immiscible fluids where the position of the interface between the fluids is of interest. In this method, a single set of momentum equations is shared by the fluid phases, and the volume fraction of each fluid phase in each computational cell is tracked throughout the domain.

A function F is defined the value of which is unity at any point occupied by one of the two fluid phases and zero otherwise. The average value of F in a cell then represents the fractional volume of the cell occupied by the considered fluid phase. The interface occurs in the cells with fractional values. As the free surface moves, the volume fractions are updated during the calculation according to an appropriate advection equation. This equation governs time dependence of F and can be written as:

$$\frac{DF}{Dt} = \frac{\partial F}{\partial t} + u\frac{\partial F}{\partial x} + v\frac{\partial F}{\partial y} + w\frac{\partial F}{\partial z} = 0 \tag{4}$$

This equation shows that the material derivative of this flow characteristic is zero, and states that F moves with the fluid.

After the computation of the volume fractions in each cell, we can define equivalent characteristics such as density and viscosity for the cell. For example, when F represents the volume fraction of the second fluid in each computational cell, then the equivalent density and viscosity of each cell can be calculated as:

$$\rho = \rho_1 + F(\rho_2 - \rho_1) \tag{5}$$

$$\mu = \mu_1 + F(\mu_2 - \mu_1) \tag{6}$$

where the subscripts 1 and 2 are related to the first and the second fluid respectively.

After finding the equivalent values of density and viscosity, the momentum equation is solved to gain the new velocity field. Eq.(4) is used to find the new volume fractions in all cells at a new time.

4 Discretization

The discretization of the above differential equations is carried out using a finite-volume approach. First, the solution domain is divided into a finite number of discrete volumes or cells, where all variables are stored at their geometric centers (see e.g. Fig.1). The equations are then integrated over all the control volumes by using the Gaussian theorem. The discrete expressions are presented regarding only one face of the control volume, namely, e for the sake of brevity.

For any variable ϕ (which may also stand for the velocity components), the result of the integration yields $\frac{\delta \upsilon}{\delta t}[(\rho\phi)_p^{n+1} - (\rho\phi)_p^n] + I_e - I_w + I_n - I_s = S_\phi \delta\upsilon$ where $I_{(s)}$ are the combined cell-face convection I^c and diffusion I^D fluxes. The diffusion flux is approximated by central differences and can be written for cell-face e of the control volume in Fig. (1) as:

$$I_e^D = D_e(\phi_p - \phi_E) - S_e^\phi \tag{7}$$

where S_e^ϕ stands for cross derivative arising from mesh non-orthogonality. A representation of the convective flux for cell-face e is:

$$I_e^c = (\rho.V.\mathrm{A})_e\phi_e = F_e\phi_e \tag{8}$$

The value of ϕ_e is not known and should be estimated by interpolation, from the values at neighboring grid

points. The expression for ϕ_e is determined by the SBIC (Djavareshkian (2001)) scheme, that is based on the NVD technique, used for interpolation from the nodes E, P and W. The expression ϕ_e for positive direction of the velocity can be written as

$$\phi_e = \phi_W + (\phi_E - \phi_W) \cdot \tilde{\phi}_e \tag{9}$$

The functional relationship used in the SBIC scheme for $\tilde{\phi}_e$ is given by:

$$\tilde{\phi}_e = \tilde{\phi}_P \quad \text{if } \tilde{\phi}_C \notin [0,1]$$

$$\tilde{\phi}_e = -\frac{\tilde{\eta}_P - \tilde{\eta}_e}{K(\tilde{\eta}_P - 1)}\tilde{\phi}_P^2 + \left(1 + \frac{\tilde{\eta}_P - \tilde{\eta}_e}{K(\tilde{\eta}_P - 1)}\right)\tilde{\phi}_P \quad \text{if } 0 \le \tilde{\phi}_P \le K \tag{10}$$

$$\tilde{\phi}_e = \frac{\tilde{\eta}_P - \tilde{\eta}_e}{\tilde{\eta}_P - 1} + \frac{\tilde{\eta}_e - 1}{\tilde{\eta}_P - 1}\tilde{\phi}_P \quad \text{if } K < \tilde{\phi}_P \le 1$$

Where

$$\tilde{\phi}_P = \frac{\phi_P - \phi_W}{\phi_E - \phi_W} \quad \tilde{\phi}_e = \frac{\phi_e - \phi_W}{\phi_E - \phi_W}$$
$$\tilde{\eta}_e = \frac{\eta_e - \eta_W}{\eta_E - \eta_W} \quad \tilde{\eta}_P = \frac{\eta_P - \eta_W}{\eta_E - \eta_W} \tag{11}$$

The limits on the K value can be determined in the following way. Obviously the lower limit is $K = 0$ which would represent switching between upwind and central differencing. This is not favorable because it is essential to avoid abrupt switching between the schemes in order to obtain solution convergence. The value of K should be kept as low as possible in order to achieve maximum resolution. The final form of the discretized equation from each approximation reads:

$$A_P.\phi_P = \sum_{m=E,W,N,S} A_m.\phi_m + S'_\phi \tag{12}$$

where $A_{(s)}$ are the convection-diffusion coefficients. The term S'_ϕ in Eq. (12) contains quantities arising from non-orthogonality, numerical dissipation terms and external sources, and $(\rho\delta\upsilon/\delta t)\phi_P$ of the old time-step/iteration level (for a time dependent equation).

5 Solution algorithm

The set of (12) is solved for the primitive variables (velocity components and energy) together with the continuity equation by means of pressure-based implicit sequential solution methods. The technique used is the SIMPLE scheme presented below. In this technique, however, the methodology has to be adapted in order to handle the way in which the fluxes are computed in Eq. (8).

The adapted SIMPLE scheme consists of a predictor and corrector sequence of steps at each iteration. The predictor step solves the implicit momentum equation using the old pressure field. Thus, for example, for the u component of velocity, the momentum predictor stage can be written as

$$u^* = H(u^*) - D\nabla p^o + S'_u \tag{13}$$

Where

$$H(u^*) = (A_E u_E^* + A_W u_W^* + A_N u_N^* + A_S u_S^*)/A_P \tag{14}$$

and

$$-D\nabla p^o = -(\frac{\partial p^o}{\partial x})_P.\delta v/A_P \equiv (-a_\eta.(p_e^o - p_w^o) + a_\zeta.(p_n^o - p_s^o))/A_P \tag{15}$$

Superscripts * and o denote intermediate and previous iteration values, respectively. Note that the pressure-gradient term is now written explicitly; it is extruded from the total momentum flux by simple subtraction and addition. The corrector-step equation can be written as

$$u^{**} = H(u^*) - D\nabla p^* + S'_u \tag{16}$$

Equations (13) and (16) can be written for the e cell-face velocities as:

$$u_e^* = \tilde{H}(u^*) - \tilde{D}\tilde{\nabla}p^o + \tilde{S}'_u \tag{17}$$

$$u_e^{**} = \tilde{H}(u^*) - \tilde{D}\tilde{\nabla}p^* + \tilde{S}'_u \tag{18}$$

Hence, from (17) and (18)

$$u_e^{**} - u_e^* = -\tilde{D}\tilde{\nabla}(p^* - p^o) \;\; or \;\; \delta u = -\tilde{D}\tilde{\nabla}\,\delta p \tag{19}$$

Now the continuity equation demands that

$$\nabla(\rho\, u^{**}) = 0 \tag{20}$$

Density is constant for incompressible flows, therefore

$$\rho u^{**} \approx \rho u^{*} + \rho \delta u \tag{21}$$

where equation (19) is invoked to eliminate δu. Substitution of (21) into (20) yields a pressure-correction equation in the form

$$A_P.\delta p_P^* = A_E.\delta p_E^* + A_W.\delta p_W^* + A_N.\delta p_N^* + A_S.\delta p_S^* + S_P \tag{22}$$

where S_P is the finite difference expression of $\nabla(\rho u^*)$, which vanishes when the solution is converged. The A coefficients in (22) take the form (the expression for A_E is given as an example)

$$A_E = \rho\,(\tilde{a}\tilde{D})_e \tag{23}$$

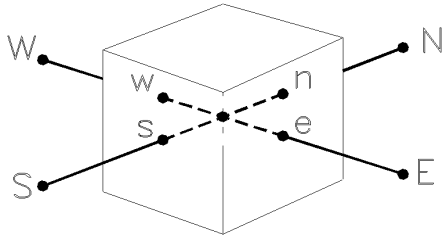

Figure 1 : Typical grid – point cluster and control volume

6 Pendulum Method

To solve the problem with an analytical method, the geometries and flow characteristics must be simplified. In the case of sloshing, the aforementioned pendulum model is a proper analytical method. In this case, it is assumed the sloshing shape can be modeled as a solid point mass oscillating around a hinge. Fig. 2 shows a circular cylinder with radius R, containing some water with depth of $R-d$. Sloshing of the water inside the cylinder can be simulated with a simple pendulum connected to the center of the cylinder with an imaginary arm with a length X_c. This length can be calculated by:

$$\begin{aligned}\int_d^R x.y.dx &= \int_d^R x.\sqrt{1-x^2}.dx = X_c.A \\ &= X_c.\int_d^R y.dx = X_c.\int_d^R \sqrt{1-x^2}.dx\end{aligned} \tag{24}$$

The general equation for pendulum oscillations reads:

$$I.\ddot{\theta} + C.R.\dot{\theta} + m.g.X_c.\theta = 0 \tag{25}$$

Where I is the second moment of area relative to center of the cylinder and C is a damping factor. These parameters read:

$$\begin{aligned}I = I_{yy} + I_{xx} = 2\rho.t.[\int_d^R x^2.\sqrt{1-x^2}.dx + \\ \int_0^{\sqrt{R^2-d^2}} y^2.(x-d).dy]\end{aligned} \tag{26}$$

Where t is the thickness of the circle (length of cylinder) and μ is the viscosity of the fluid. The initial conditions for the above mentioned oscillation equation are:

$$\theta|_{t=0} = \theta_0 \tag{27}$$

$$\dot{\theta}\big|_{t=0} = 0 \tag{28}$$

Where θ_0 is the initial free surface angle and it depends on the centrifugal and gravity accelerations. The equation (25)

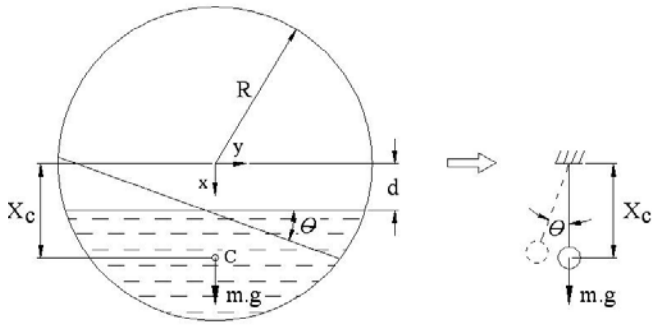

Figure 2 : Sloshing in a half-empty cylinder

is solved with the Runge-Kutta method and θ is calculated at each time step. By finding the free surface angle at each time step, it is clear that the horizontal force exerted on the wall by the liquid, is the x-component of the total force calculated by multiplying the hydrostatic pressure by the wetted area, therefore the horizontal force due to sloshing can be obtained at each time step.

7 Result

The results of the numerical simulations based on the finite volume method with the VOF technique, and the pendulum models are compared for a tanker truck having a circular cross-section with one unit in diameter. A

tanker-truck with a horizontal circular cylinder and 4m of length in the axial direction moving in a road with a velocity of 10m/s is considered. The road has a circular shape with 250m radius. Two different accelerations are applied to the system, gravity and centrifugal accelerations. Before the tanker enters the curved road, vertical gravity is the only component of acceleration and then at time t=0 a horizontal acceleration is added to the system and thus sloshing occurs.

The series of frames in Fig. 3 shows the results obtained using both the VOF method (solid line) and the analytical method (dotted line) for water elevation of 0.35, 0.25, 0.15 and 0.05 m measured from the center of the tanker. The results of these two methods have also been compared with those of the Finite-Element method from the numerical work of Aliabadi et al. (2003). In Fig. 3, the circles show the cross-section of the tanker and the elevation of the water.

As expected, both methods have relatively good agreements when the water inside the tanker is low (d=0.35). The frequency of the sloshing is almost the same for all methods at low and moderate amount of the water inside the tanker (d=0.35 and d=0.25m). The differences between amplitude and frequency of sloshing provide by different methods become large when there is a significant amount of water inside the tanker (d=0.05).

In this paper, the effect of the geometry of the tanker on the results is also investigated. For this purpose, the above mentioned tanker truck with a circular cross-section with 1m diameter is compared with another tanker with the cross section of an ellipse with minor and major diameters of 1m and 1.33m respectively. This comparison shows differences in results due to the shape of the tanker. To show the effect of tanker size, another elliptic tanker with 1.5 times larger dimensions (1.5m for minor dia. and 2m major dia.) has been compared with these two tankers. All these tanker-trucks with 4m length are moving in a road with a velocity of 10m/s. The road has a circular shape with a radius of 250m. Fig. 4 shows the results obtained for these different tankers for water elevation of 0.35, 0.25, 0.15 and 0.05 m measured from the center of the tanker.

It is clear that the amplitude of the force is increased with increasing the cross section area of the tanker and its contained liquid. But the frequency of the sloshing is decreased for the larger tankers and liquid amount. Also comparison of the results in Fig. 4 shows that the fre-

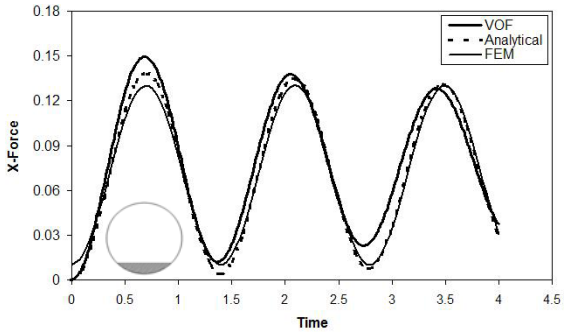

a) d=0.35

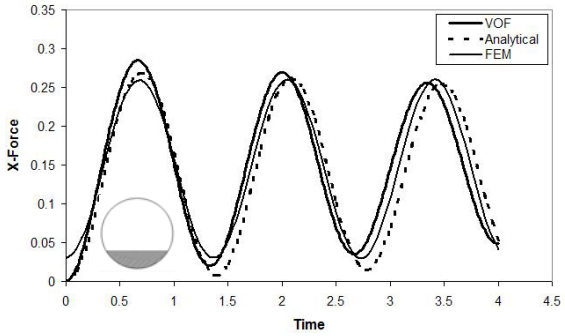

b) d=0.25

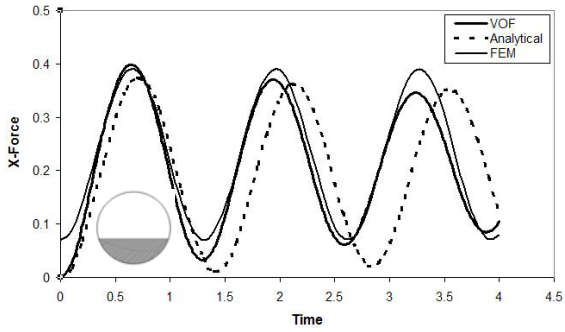

c) d=0.15

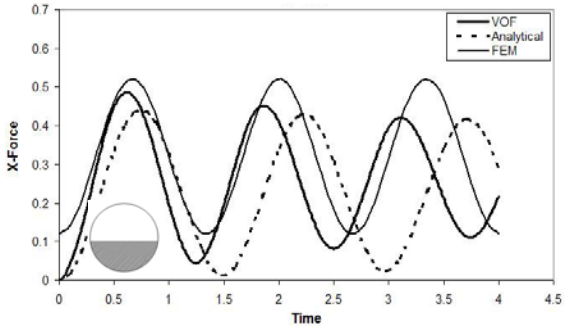

d) d=0.05

Figure 3 : Horizontal force applied to the tanker for different methods

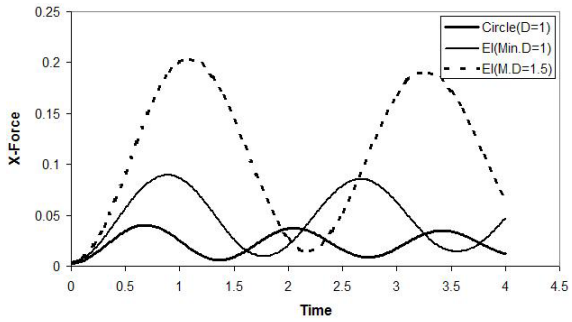

a) d=0.35

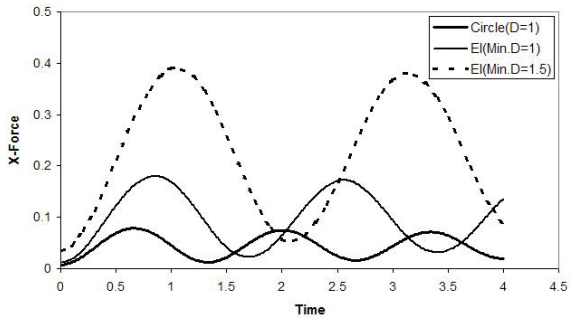

b) d=0.25

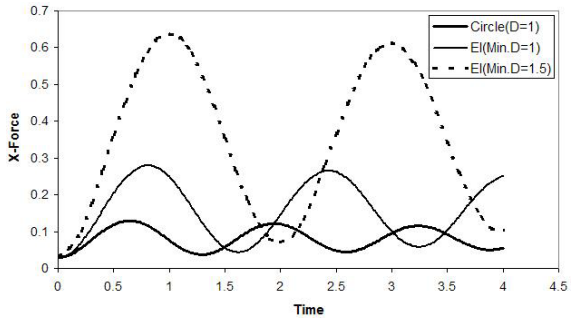

c) d=0.15

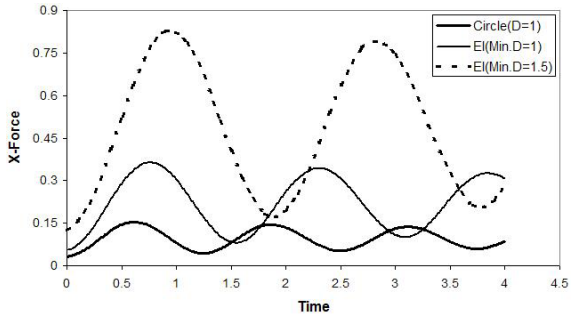

d) d=0.05

Figure 4 : Horizontal force applied to the tanker for different geometries

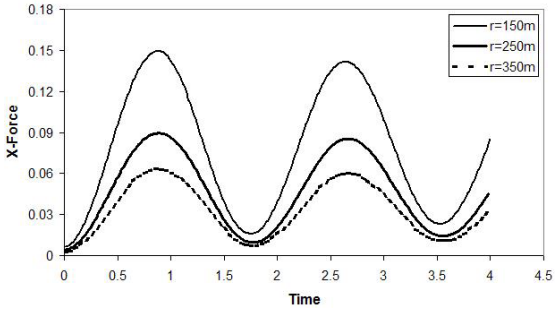

a) d=0.35

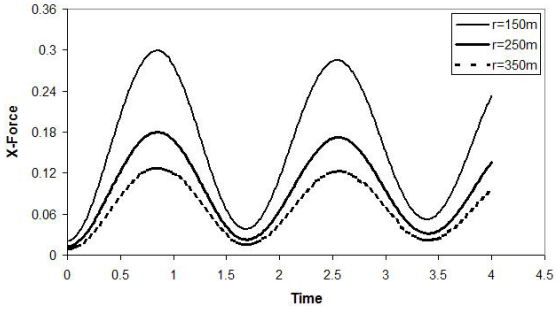

b) d=0.25

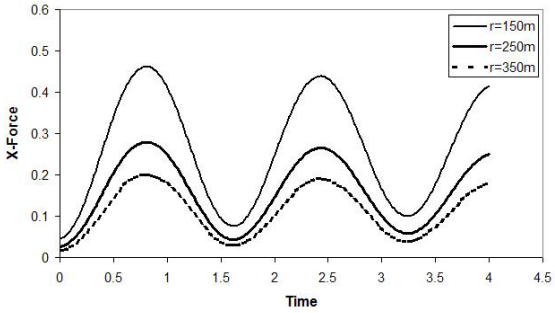

c) d=0.15

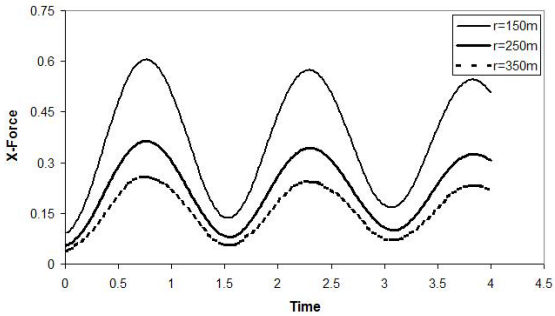

d) d=0.05

Figure 5 : Horizontal force applied to the tanker for different radii of the road

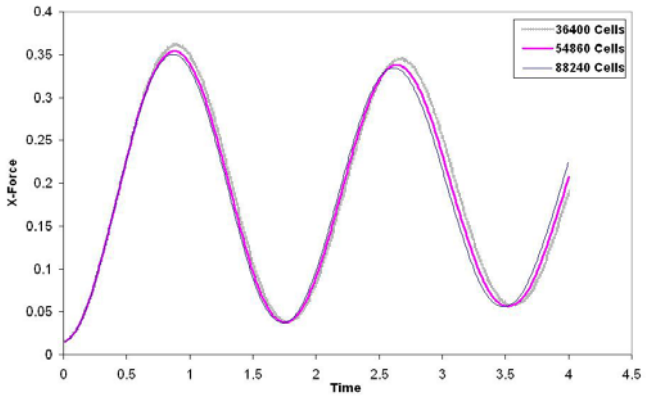

Figure 6 : Grid independence test

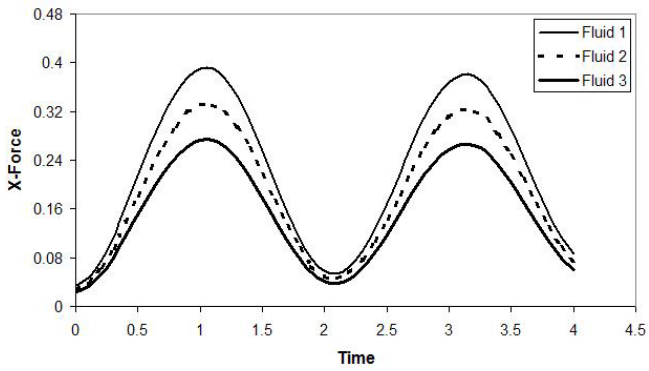

Figure 7 : Horizontal force applied to the tanker for fluids with different densities

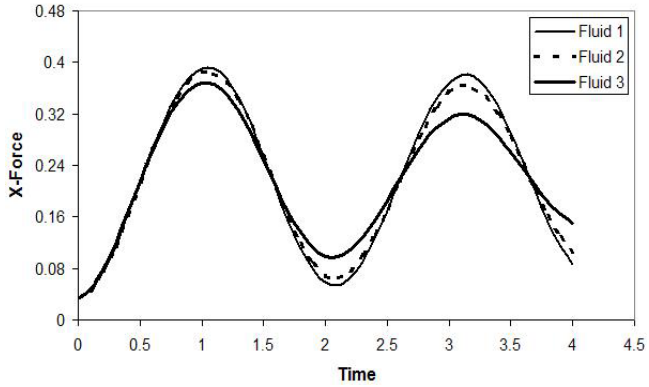

Figure 8 : Horizontal force applied to the tanker for fluids with different viscosities

quency of sloshing for all tanker geometries is increased by decreasing the water depth in the tanker.

The effect of different physical conditions due to different road curves on the results is also investigated. For this purpose, a horizontal tanker is considered with the cross section of an ellipse with minor and major diameters of 1m and 1.33m respectively. This tanker is entering roads with 150m, 250m and 350m radius. This comparison shows differences in results due to the radius of road. The tanker-truck with 4m of length is moving in each road with a velocity of 10m/s. Fig. 5 shows the results obtained for these different roads with water elevation of 0.35, 0.25, 0.15 and 0.05 m measured from the center of the tanker.

It is clear that the amplitude of the force is increased with increasing the water depth in the tanker. But the frequency of the sloshing is constant for each set of diagrams and does not change for different road curves. Also comparison of the results in Fig. 5 shows that the frequency of sloshing for all road radii increases when the water depth in the tanker decreases.

A grid independence test for the simulation of a tanker truck having an ellipse cross-section with minor and major diameters of 1m and 1.33m respectively is shown in Fig. 6. A tanker-truck with a 4m of length in the axial direction moving in a road with a velocity of 10m/s is considered. The road has a circular shape with 250m radius. The results for different meshes change slowly. This indicates that an acceptable solution can be obtained on the grid 36400 cells.

The last part of this study is about the effects of different liquid properties on the sloshing phenomena in the tanker. For this purpose, another tanker is assumed with the cross section of an ellipse with minor and major diameters of 1.5m and 2m respectively. This tanker is entering a road with 250m radius and the distance between free surface and center of ellipse in all cases is d=0.25D where D is the minor diameter(1.5m).

In a first case, three fluids with densities 1200, 1000 and 800 kg/m^3 are assumed respectively. The comparison of the results in Fig. 7 shows differences due to the different densities. It is obvious that the amplitude of the force increases, when the liquid density in the tanker increases, since the force depends on the liquid weight and its density.

In a second case, three fluids which have the same density of water (1000 kg/m^3) with viscosities of 0.001 kg/m.s (viscosity of water), 0.1 and 10 kg/m.s are assumed respectively. The comparison is done in Fig. 8 and shows differences in results due to different viscosities. This figure shows that the amplitude of the force does not de-

pend on the viscosity of the liquid and viscosity only affects the damping and the end time of sloshing in the tanker.

8 Conclusion

In this paper, a finite volume, VOF method has been used to simulate typical sloshing phenomena in containers. The results of these simulations have been compared with a simple pendulum model and FEM results. The main findings can be summarized as follows: 1- For sloshing applications in tanker trucks during turning, the results obtained from these methods are qualitatively comparable for low and moderate amount of the fuel or water inside the tanker. On the other hand, in the presence of a significant amount of liquid inside the tanker, the models lead to different solutions. 2- The amplitude of the force is increased with increasing the cross section area of the tanker and its contained liquid, but the frequency of the sloshing is decreased for the larger tankers and liquid amount. 3- The frequency of sloshing for all road radii is increased with decreasing the water depth in the tanker. 4- The amplitude of the force is increased with increasing the liquid density in the tanker. 5- The amplitude of the force does not depend on the viscosity of liquid, and viscosity only affects the damping and the sloshing end time.

References

Abramson, H.N. (1966): The Dynamics Behavior of Liquids in Moving Containers, NASA, SP-106, *South West Research Institute for the National Aeronautics and Administration*

Aliabadi, S. and Tezduyar, T. (2000): Stabilized-finite-element/interface-capturing technique for parallel computation of unsteady flows with interfaces, *Compt. Method Appl. , Mech. Engg*. vol. 190, pp. 243-261

Aliabadi, S., Johnson, A., and Abedi, J., (2003): Comparison of Finite Element and Pendulum Models for Simulation of Sloshing, *Elsevier, Computers & Fluids* vol. 32, pp. 535-543

Amabili, M., (1996): Free Vibration of Partially Filled, Horizontal Cylindrical Shells, *Journal of Sound and Vibration*, vol. 191(5), pp. 757-780

Deville, M.O., (1974): Numerical Experiments on the MAC Code for a Slow Flow, *J. Comp. Phys*. vol. 15, pp. 362-374

Djavareshkian, M.H. (2001): A New NVD Scheme in Pressure-Based Finite-Volume Methods. 14^{th} *Australasian Fluid Mechanics conference*, Adelaide University, Adelaide, Australia, pp. 339-342

Esmaeeli, A., (2005): Phase Distribution of Bubbly Flows under Terrestrial and Microgravity Conditions, *FDMP: Fluid Dynamics & Materials Processing,* vol. 1(1): pp. 63-80.

Hirt, C.W., and Shannon, J.P., (1968): Free-Surface Stress Conditions for Incompressible Flow Calculations, *J. Comp. Phys.* vol. 2, pp. 403-411

Hirt, C.W., Nichols, B.D., and Romero, N.C., (1975): SOLA-A Numerical Solution Algorithm for Transient Fluid Flows, *Los Alamos Scientific Laboratory Report* LA-5852

Hirt, C.W. and Nichols, B.D., (1981): Volume Of Fluid (VOF) Method for the Dynamics of Free Boundaries, *J. Comp. Phys.* vol. 39, pp. 201-225

Hogea, C.S., Murray B.T., Sethian J.A., (2005): Implementation of the level set method for continuum mechanics based tumor growth models, *FDMP: Fluid Dynamics & Materials Processing,* vol. 1(2): pp. 109-130.

Jimènez, E., Sussman M., and Ohta M, (2005): A Computational Study of Bubble Motion in Newtonian and Viscoelastic Fluids, *FDMP: Fluid Dynamics & Materials Processing,* vol. 1 (2): pp. 97-108.

Johnson, A. and Aliabadi, S., (2000): Application of automatic mesh generation and mesh multiplication technique to very large scale free-surface flow simulations, *Proceeding of the 7^{th} International Conference on Numerical Grid Generation in Computational Field Simulations*, Whistler, Biritish Columbia, Canada, September 25-28

Lappa, M., (2005a): Coalescence and non-coalescence phenomena in multi-material problems and dispersed multiphase flows: Part 2, a critical review of CFD approaches, *FDMP: Fluid Dynamics & Materials Processing,* vol. 1(3): pp. 213-234.

Liu Jun, (1985): Application of Variable Blockage Method to Steady Flows over Curved Beds, C.F.D.U. *Report CFD/85/12*, Imperial College

Liu Jun, (1986): Computer Modeling of Flows with a Free Surface, *Thesis for PHD*., Univ. of London, CFDU

Martin, J.C. and Moyce, W.J., (1952): An Experimental Study of the Collapse of Liquid Columns on a Rigid

Horizontal Plane, *Phil. Trans. Roy. Soc. London*, no. 244, pp. 312-324

Maxwell, T.T., (1977): Numerical Modeling of Free-Surface Flows", *PhD Thesis, University of London*

Nichols, B.D. and Hirt, C.W., (1971): Improved Free Surface Boundary Conditions for Numerical Incompressible-Fluid Calculations, *J. Comp. Phys.* vol. 8, pp. 434-448

Nichols, B.D. and Hirt, C.W., (1975): Methods for Calculating Multidimensional Transient Free Surface Flows Past Bodies, *Los Alamos Scientific Laboratory Report* LA-UR-75-1932

Warnitchai, P. and pinkaew, T., (1998): Modeling of Liquid Sloshing in rectangular Tanks with Flow-Dampening Devices, *Elsevier, engineering structures*, vol. 20, no. 7, pp. 593-600